Biophysical Chemistry, 38 (1990) 23–32
Elsevier

BIOCHE 01455

Dissociation of *Limulus polyphemus* (horseshoe crab) hemocyanin

I. Solution X-ray scattering study in equilibrium *

Kazumoto Kimura [a], Yoshihiko Igarashi [b], Akihiko Kajita [b], Zhi-Xin Wang [c], Hirotsugu Tsuruta [d], Yoshiyuki Amemiya [e] and Hiroshi Kihara [f]

[a] *Division of Medical Electronics and* [b] *Department of Biochemistry, Dokkyo University School of Medicine, Mibu, Tochigi 321-02, Japan,* [c] *Laboratory of Molecular Enzymology, Institute of Biophysics, Academia Sinica, Beijing 100080, P.R. China,* [d] *Department of Materials Science, Faculty of Science, Hiroshima University, Hiroshima 730,* [e] *Photon Factory, National Laboratory for High Energy Physics, Tsukuba 305 and* [f] *Jichi Medical School, School of Nursing, Minamikawachi, Tochigi 329-04, Japan*

Received 18 November 1989
Revised manuscript received 19 February 1990
Accepted 5 March 1990

Solution X-ray scattering; Hemocyanin; Dissociation; Ca^{2+}; (*Limulus polyphemus*)

A solution X-ray scattering study has been performed on *Limulus polyphemus* (horseshoe crab) hemocyanin and its dissociated fragments at various pH values in the presence and absence of Ca^{2+}. The scattering patterns of native hemocyanin (48-mer), the half molecule (24-mer), quarter molecule (12-mer) and monomer fraction were measured. The radii of gyration for the four molecular species were calculated from the Guinier plots to be 110.7, 91.3, 77.3, and 36.5 Å, respectively. Models which yield good fits to the experimental data are presented. The models were constructed using eight, four and two spheres with a radius of 58 Å, assuming the sphere to be the submultiple composed of six subunits. The radii of gyration were calculated on the basis of the model and the values found to be 106, 94 and 73 Å, respectively, in good agreement with the experimental results.

1. Introduction

Limulus polyphemus hemocyanin is an oxygen carrier protein of molecular mass 3.6 MDa. This hemocyanin consists of 48 subunits, which are assembled to build eight submultiples. The submultiple which comprises six subunits is also called the basic hexameric unit or hexameric building block [1]. Extensive ultracentrifugation studies carried out by Brenowitz et al. [2] led to the observation of the native hemocyanin (48-mer) dissociating into low molecular mass fragments depending on the pH and Ca^{2+} concentration. The fact that the hemocyanin dissociates into the 24-mer on removal of Ca^{2+} at physiological pH and into the 12-mer at pH 5.0 is of particular interest from structural and functional points of view, since native hemocyanins of similar size have been found to occur in the arthropods, e.g., *Androctonus australis* (24-mer), *Astacus leptodactylus* (12-mer), *Panulirus interruptus* (6-mer), etc.

In the meantime, unique models for the quaternary structure of the arthropodan hemocyanin occurring in nature have been proposed by Lamy et al. [1] on the basis of molecular immunoelectron microscopy. However, details of the

Correspondence address: K. Kimura, Division of Medical Electronics, Dokkyo University School of Medicine, Mibu, Tochigi 321-02, Japan.

* This work has been performed under the approval of the Photon Factory Program Advisory Committee (Proposal nos 85-117 and 88-060).

steric arrangement of their submultiples remain to be established. Consequently, we considered further investigation of the structure of native hemocyanin and particularly of the dissociated fragments by means of a different approach to be a pertinent objective for our research efforts.

The technique of solution X-ray scattering (SXS) is a useful tool for gaining information on the gross conformation of macromolecules [3]. In fact, its usefulness has been demonstrated by Pilz et al. in the analysis of quaternary structure of hemocyanins from *A. leptodactylus* [4] and *Helix pomatia* [5], and of hemoglobins from *Helisoma trivolvis* [6] and *Tylorrhynchus heterochaetus* [7].

The present study is aimed at the investigation of the gross conformations of native hemocyanin from horseshoe crab and its dissociated fragments by the SXS technique along the lines mentioned above. The kinetics of the process of dissociation can also be followed with the stopped-flow X-ray scattering (SFXS) method [8,9] (results to be published elsewhere).

2. Materials and methods

Hemolymph from horseshoe crab (*L. polyphemus*) was provided by Dr H. Sugita (Tsukuba University). Hemocyanin was purified according to the method of Brenowitz et al. [2], which was conducted at 4°C throughout, unless otherwise stated. The 60 S hemocyanin obtained from hemolymph as the pellet resulting from ultracentrifugation at 225 000 × *g* for 60 min was dissolved in 50 mM Tris-HCl, pH 7.4, containing 10 mM $CaCl_2$. The hemocyanin solution was dialyzed for 24 h against Tris-HCl buffer ($I = 0.15$), pH 7, containing either 10 mM $CaCl_2$ or 20 mM EDTA for use as the intact native molecule or half molecule (24-mer), respectively. The quarter molecule (12-mer) was prepared by dialysis for 24 h against acetate buffer ($I = 0.15$), pH 5, in the presence of 20 mM EDTA. The monomer was obtained by mixing native hemocyanin with Tris-HCl buffer, pH 9 (final $I = 0.1$) containing 50 mM EDTA and allowing the mixture to stand for 12 h at room temperature. Purity of the dialyzed samples was assessed by sedimentation analysis at 20°C using a Hitachi 282 analytical ultracentrifuge. The native species and the 24-mer were demonstrated to be homogeneous by ultracentrifugation, giving rise to a single peak of 60 S and 38 S, respectively. The dodecamer was found to be somewhat heterogeneous, showing a minor peak of 27 S (7.7%) in addition to a major peak of 23 S (92.3%), while the monomer appeared to be substantially homogeneous with a single peak of 5.7 S. From these preliminary experiments, all of the specimens were regarded as consisting of a single component from a practical point of view in spite of minor contamination in the case of the quarter molecule and were therefore subjected to X-ray scattering analysis. Hemocyanin concentration was determined using an extinction coefficient ($E^{1\%}_{1cm}$) of 13.04 at 280 nm or 3.31 at 340 nm as reported by Brouwer et al. [10].

X-ray scattering experiments were performed at the beam line 15A1 of the Photon Factory, National Laboratory for High Energy Physics. The camera and detection systems have been reported in detail elsewhere [11]. In this experiment, the sample solution was irradiated with monochromatic X-rays (1.504 Å) and scattered X-ray intensities were recorded on a position-sensitive proportional counter (PSPC) (512 channels) with a camera length of 2412 mm and channel width of 0.368 mm. The central part of the PSPC was covered with 6 mm lead sheet in order to avoid the effect of unscattered light. For all X-ray scattering measurements correction of scattered X-ray intensities was performed in order to cancel out the effect of the intensity decay of the incident X-ray beams by means of the ionization current of an ion chamber placed in front of the sample cell. The scattering data were normalized with respect to exposure time and protein concentration. Normalized data were also subjected to background subtraction. X-ray scattering data were expressed in terms of $h = 4\pi \sin\theta/\lambda$ (λ, wavelength; 2θ, scattering angle) and the R_g value was determined from the slopes of Guinier plots [12] prior to commencing the model analysis.

Model analyses were carried out on the basis of the program developed by Furuno et al. [13]. The software systems were modified to fit an NEC PC9801 microcomputer with some improvement

in the resolution for calculation. Data recorded in the SXS measurements were first stored in a PDP11 and then transferred to a micro-VAX II. Analyses were performed according to the least-squares method developed by Kimura (unpublished data). $P(r)$, the pair distance distribution function, was calculated from the experimental results with the following equation [14]:

$$P(r) = \frac{1}{2\pi^2} \int_0^\infty I(h)(hr) \sin(hr)\, \mathrm{d}h$$

Desmearing was omitted, since the effect of smearing was insignificant for experiments conducted at the Photon Factory [15].

3. Results and discussion

3.1. Solution X-ray scattering in equilibrium

SXS data on hemocyanin were evaluated at pH 7.0 in the presence and absence of 20 mM EDTA. Figs 1a and 2a (continuous traces) show final scattering curves recorded in the absence and presence of 20 mM EDTA, i.e., conditions under which the native protein (48-mer) and the half-molecule (24-mer) of hemocyanin are expected to exist, respectively. The scattering curve in the absence of EDTA (native state) displays two minima at $h = 0.034$ and 0.078 Å^{-1} and three maxima at $h = 0$, 0.045 and 0.108 Å^{-1}. The prominent subsidiary maxima reflect the high degree of symmetry of the macromolecule in solution. In the case of the pattern in the presence of EDTA (D_1 state), however, the first minimum and second maximum are replaced by a shoulder, while the second minimum and third maximum remain unchanged, indicating the existence of some degree of symmetry of the protein as compared to the native form.

The radius of gyration, R_g, at zero concentration of hemocyanin was estimated as follows. The scattering intensity at each PSPC channel was normalized with respect to the ion chamber current (100 nA standard), and to the concentration of protein (1 mg/ml standard). The logarithm of the normalized intensity was then extrapolated to zero protein concentration, thereby yielding the values for the normalized intensities at [protein] = zero for each PSPC channel. R_g and the zero-angle intensity, I_0, were evaluated from Guinier plots of the normalized scattering curve at zero [protein] in the region of $hR_g < 1$. The values of I_0

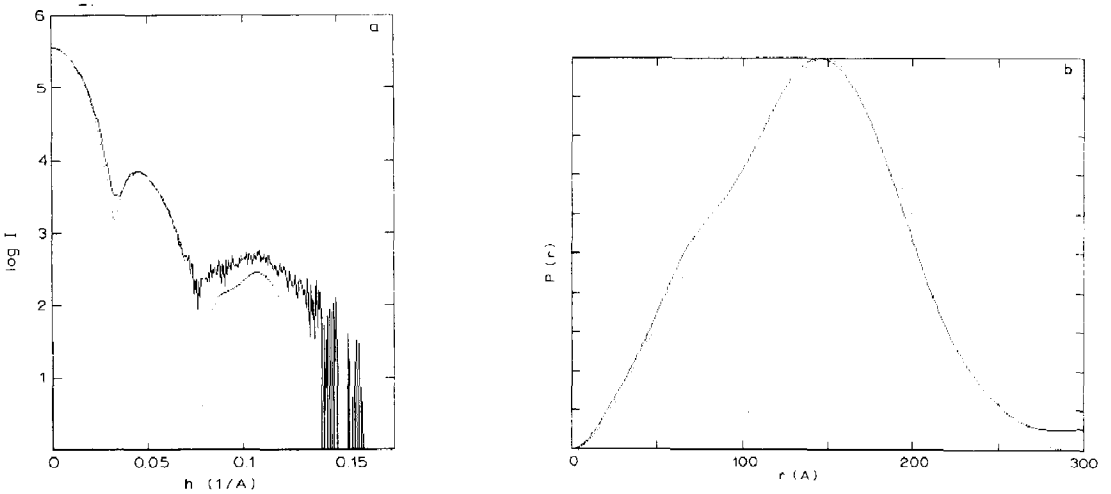

Fig. 1. (a) X-ray scattering pattern of native hemocyanin from *L. polyphemus* (———) compared with that calculated on the basis of the model B (· · · · · ·). $\lambda = 1.504$ Å; exposure time, 100 s; intensity is normalized to a value of 100 nA. (b) $P(r)$ function of native hemocyanin from *L. polyphemus* calculated from the experimental results (———) and simulated curve according to model B (· · · · · ·).

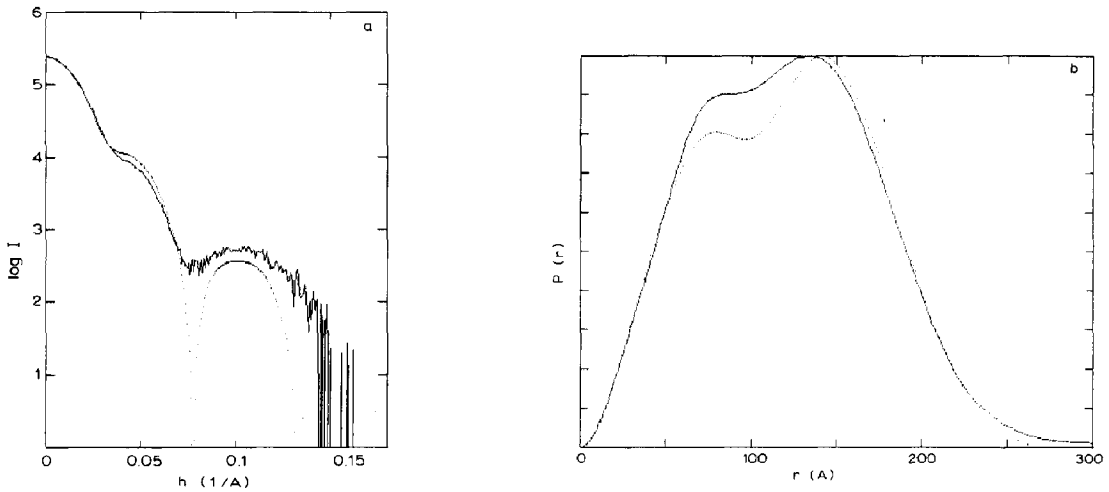

Fig. 2. (a) Comparison of the X-ray scattering pattern of *L. polyphemus* hemocyanin (D_1 state) in the presence of 20 mM EDTA at pH 7 (———) with that calculated according to model D (· · · · · ·). Conditions: identical to those in fig. 1a, except pH and EDTA. (b) $P(r)$ functions of *L. polyphemus* hemocyanin (D_1 state) calculated from the experimental results (———), in comparison with that of model D (· · · · · ·).

and R_g thus obtained for the native species and dissociated fragments are listed in table 1. The results are in excellent agreement with those obtained conventionally, as extrapolated to zero concentration of protein (Kimura et al., unpublished data). A typical Guinier plot is shown in fig. 3.

The SXS pattern of hemocyanin was also recorded at pH 5.0 in the presence of 20 mM EDTA (D_2 state). The results are depicted in fig. 4a, a minimum at $h = 0.078$ Å^{-1} and a maximum at $h = 0.108$ Å^{-1} being observed. The minima in figs 2a and 4a, and the second minimum of fig. 1a are

Table 1

Zero-angle Intensity (I_0) and radius of gyration (R_g) of *L. polyphemus* hemocyanin and its dissociated fragments at various protein concentrations

Hemocyanin (%)	I_0 (counts/s)			R_g (Å)			
	pH 7 with 10 mM $CaCl_2$ (native) (48-mer)	pH 7 with EDTA (D_1 state) (24-mer)	pH 5 with EDTA (D_2 state) (12-mer)	pH 7 with 10 mM $CaCl_2$ (native) (48-mer)	pH 7 with EDTA (D_1 state) (24-mer)	pH 5 with EDTA (D_2 state) (12-mer)	pH 9 with EDTA (D_3 state) (monomer)
0.25	948.4	–	–	110.30	–	–	–
0.5	1822	1051	556	110.67	91.50	78.49	–
1.0	4472	1997	1137	110.31	92.72	81.24	–
1.5	4475	2805	1797	110.31	92.78	86.33	–
2.0	5476	3520	2170	109.66	93.06	83.46	–
2.7	–	–	–	–	–	–	36.5
EV [a]	4119	2128	1275	110.67	91.32	77.32	
SD [b]	±79	±39	±34	±1.24	±1.42	±2.36	

[a] Evaluated value, determined from the pattern at zero concentration.
[b] Standard deviation of I_0 and R_g.

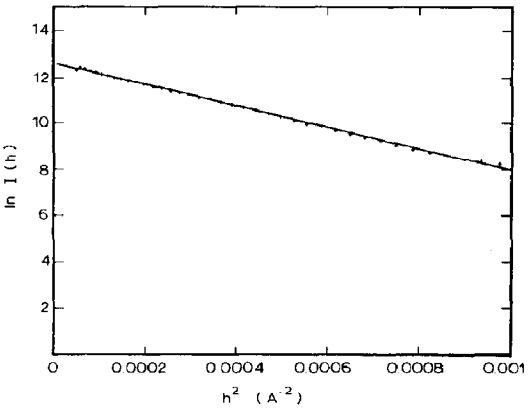

Fig. 3. A typical Guinier plot of SXS data for native hemocyanin from *L. polyphemus*.

at the same position with respect to the h value. This is also the case for the maxima of figs 2a and 4a ($h = 0.078$ Å^{-1}) and the third maximum of fig. 1a ($h = 0.108$ Å^{-1}).

The R_g values of the three molecular species (native, D_1 and D_2) of hemocyanin were calculated to be 110.7, 91.3 and 77.3 Å, respectively, from the Guinier plot. Subsequent evaluation of R_g raised to the third power should result in a ratio of $1:1/2:1/4$, when the three molecular species of hemocyanin are assumed preliminarily to correspond to a large sphere. On the other hand, the ratio determined on the basis of the experimental curves was found to be $1:1/1.8:1/2.9$. The significant discrepancy between the R_g values, especially of the D_2 state, provides a direct indication of the above-mentioned approximate models being clearly inadequate, consequently necessitating detailed model analysis, as described in subsequent sections.

The SXS pattern of the hemocyanin fragment was also monitored at pH 9.0 in the presence of 10 mM EDTA (D_3 state) at a protein concentration of 2.7%. The scattering intensity was much lower compared to the other three (fig. 5a). The R_g values were estimated from Guinier plots and are listed in table 1 together with those for the other cases. The ratio of R_g^3 of the native form to that of the D_3 state amounted to $1/27.9$, thus confirming that the protein dissociates mainly into the monomer at pH 9.0 in the presence of EDTA.

As demonstrated by the data in table 1, the R_g values of the native and D_1 state exhibit very little dependence on the protein concentration, whereas that of the D_2 state was moderately affected. The fact that the radius of gyration (12-mer) varied with concentration suggests that some form of

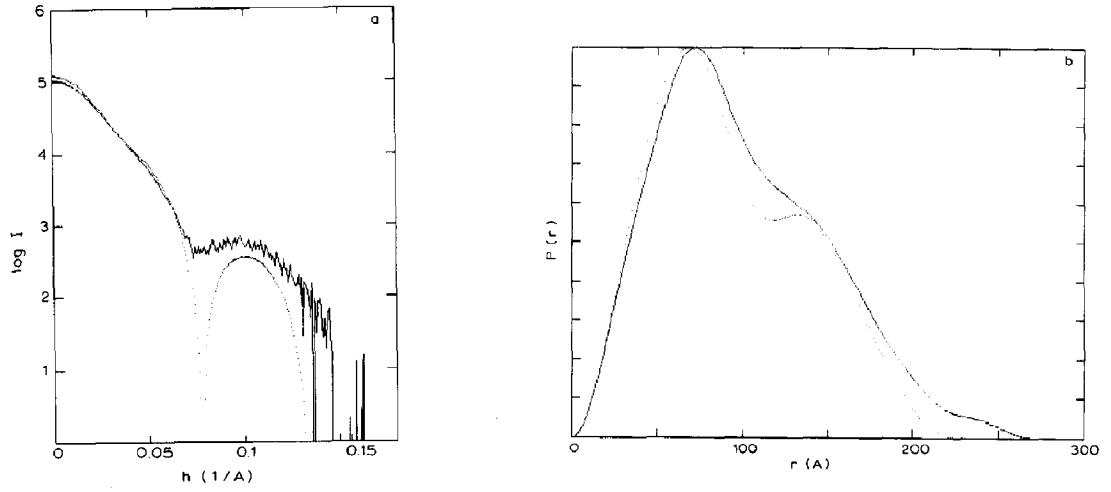

Fig. 4. (a) X-ray scattering pattern of *L. polyphemus* hemocyanin (D_2 state) in the presence of 20 mM EDTA at pH 5 (———) compared with that calculated for model E (· · · · · ·). Conditions: same as in fig. 1, except pH. (b) $P(r)$ functions of *L. polyphemus* hemocyanin (D_2 state) calculated from the experimental results (———) compared with that of model E (· · · · · ·).

interaction, such as association, took place between molecules of the dodecamer in solution.

The function $P(r)$ was evaluated for the four molecular species and is plotted in figs 1b, 2b, 4b and 5b, respectively. The $P(r)$ functions will be discussed later.

3.2. Model analyses

Model analyses were performed based on the fact that the native protein (48-mer) and its dissociated fragments (24-mer and 12-mer) are composed of eight, four and two submultiples, respectively. The overall shape of the native hemocyanin molecule (48-mer) was approximated by the two models designated A and B, each of which consists of eight submultiples arranged in the form of two superimposed tetragonal layers (fig. 6a), assuming each submultiple to be a sphere for the sake of simplicity, as follows.

Model A: eight submultiples are placed with one submultiple at each corner of a cube, and in contact with three neighboring submultiples. That is, the four submultiples of the upper layer are directly above the four of the lower layer.

Model B: the upper layer of model A is rotated through 45° to result in a staggered configuration with respect to the lower layer so that each of the upper submultiples is located at a position intermediate between those corresponding to the two lower submultiples (see fig. 6a).

Based on the appearance of native hemocyanin from *L. polyphemus* shown in the electron micrographs reported by Lamy et al. [1], we determined the radius of a submultiple (hexameric building block) to be about 60–70 Å. We then calculated the scattering patterns for models A and B by altering the radius of a submultiple R_0. In fig. 7a, scattering patterns for the two models are illustrated using a value for R_0 of 58 Å. This value was found to yield the best fit to the experimental results as described below.

Comparison of the theoretical curves calculated from models A and B (fig. 7a) clearly indicates that the first and second maxima as well as the first and second minima are in fairly good agreement with each other as regards either position or height, whereas the profile of the third maximum is significantly different. As is evident from the dotted line in either fig. 1a or fig. 7a, on the whole, model B results in a closer fit to the experimental curve than does model A (fig. 7a, continuous line).

We also calculated the scattering pattern of the 48-mer on the basis of a cylindrical model where eight cylinders (116 Å diameter, 116 Å height) are

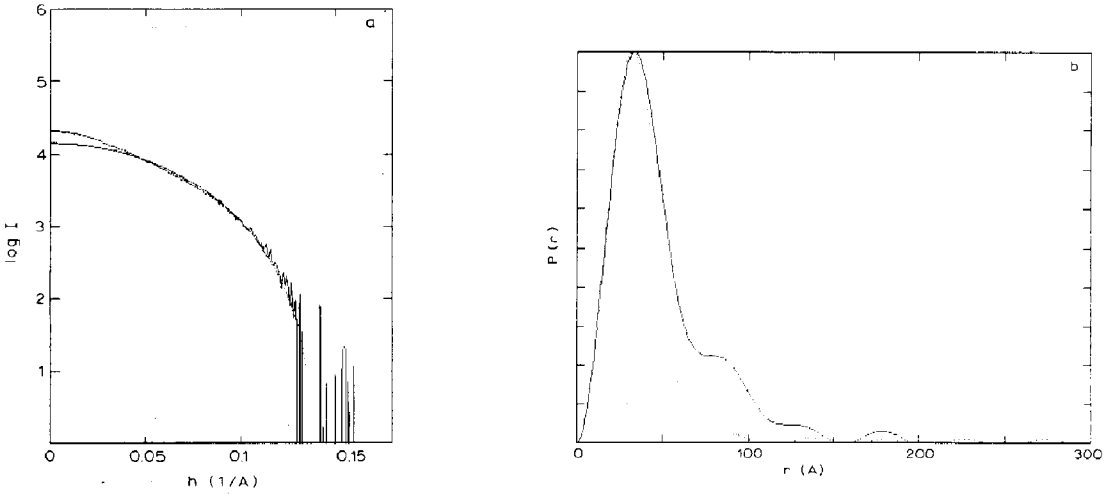

Fig. 5. (a) X-ray scattering pattern of *L. polyphemus* hemocyanin (D_3 state) at pH 9.0 in the presence of 20 mM EDTA (———). (b) $P(r)$ functions of *L. polyphemus* hemocyanin (D_3 state). Experimental results (———).

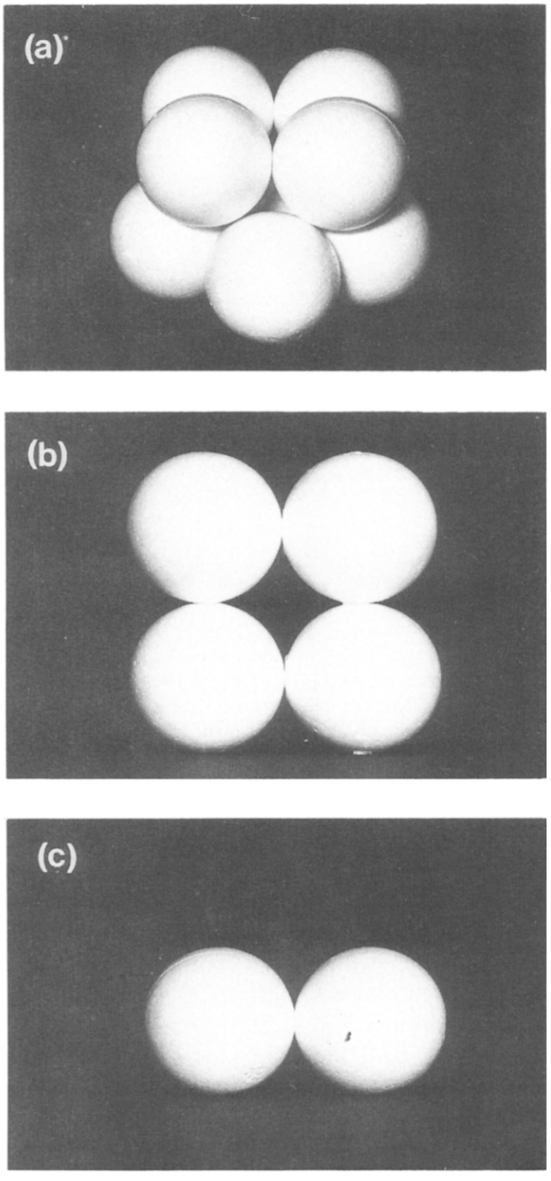

Fig. 6. Ping-pong ball models of *L. polyphemus* hemocyanin. (a) Native form (48-mer), model B; (b) 24-mer, model D; (c) 12-mer, model E.

aligned so that the center of each cylinder is located at the corner of a cube. The calculated curve displays a fine structure around the second maximum, which was not observed in the experimental pattern. For this reason, the cylindrical model was considered to be less plausible.

The scattering patterns for the 24-mer were also calculated according to the following two models.

Model C: a tetrahedron composed of four submultiples.

Model D: four submultiples are located in a layer as is presumed for both upper and lower layers of models A and B (see fig. 6b).

Taking 58 Å as the radius of the submultiple (R_0), model calculations were performed. As shown in fig. 7b, the first shoulder of model C shows a deeper cleft than that of model D, although the overall profile is not markedly different.

We then performed a fit of the 48-mer using model B. The simulated curve is depicted in fig. 1a in comparison with that obtained experimentally. The R_g value calculated from the model was found to be 106 Å, which is comparable with the experimental results (110.7 Å). The calculated curve for model B displays maxima and minima at identical positions to those of the experimental curve, indicating a good fit of the model. The minima for the experimental curve are not as deep when compared with the case for the model calculations. The ratio of the first shoulder to the first maximum is also consistent between both curves.

With regard to the 24-mer, both models (C and D) appear to fit the experimental curves equally well, insofar as the profile is concerned (figs 2a and 7b). The difference between the two models is the height of the shoulder around $h = 0.05$ Å^{-1}. Another feature distinguishing between the two models is the radius of gyration as evaluated from the models; $R_g = 84$ Å (model C) and $R_g = 93.5$ Å (model D). Concerning the profile of the scattering curve, model D yields a better fit to the experimental data than does model C, particularly with respect to the shoulder around $h = 0.04$ Å^{-1}. The R_g value of model D (93.5 Å) appears to be very close to that obtained experimentally (91.3 Å). However, comparison of the R_g ratio given above for the 24-mer vs the 48-mer based on model D (1 : 1/1.46) with the value obtained in experiments (1 : 1/1.8) demonstrates that the R_g value of model D is greater than the experimental

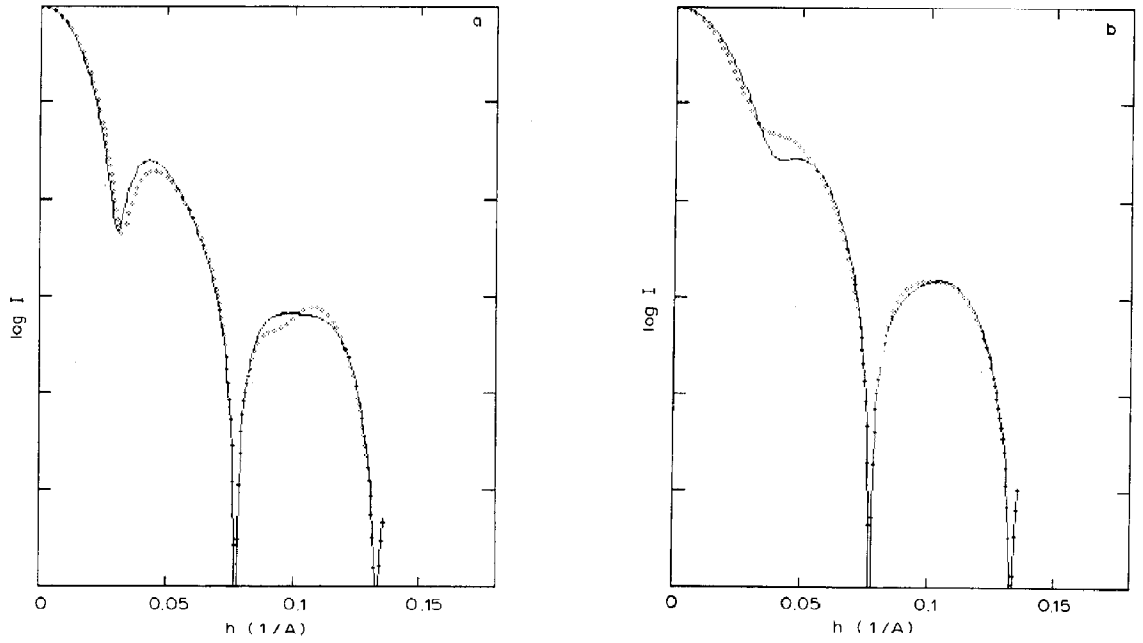

Fig. 7. Scattering patterns calculated from: (a) model A for 48-mer (———). 58 Å was used as the radius of each submultiple. Each submultiple is placed at the corners of a cube and is in contact with three neighboring submultiples. Model B for 48-mer (· · · · · ·). The four upper submultiples of model A have been rotated through 45° (see fig. 5a). (b) Model C for 24-mer (———), four submultiples closely packed as a tetrahedron. Model D for 24-mer (· · · · · ·), four submultiples in-plane (see fig. 6b).

value. This might be attributable to the occurrence of a conformational change, e.g., a slight twist in the two dodecamer (dimeric submultiples). In fig. 2a, the simulated curve according to model D is depicted together with that from the experiments. Although the ratio of the first shoulder to the first minimum is different, albeit to a lesser degree, both curves agree well within the experimental precision.

Simulated $P(r)$ functions for models B and D are shown together with the corresponding experimental data in figs 1b and 2b. Good agreement is observed between the simulated curves and the experimental profiles. In fig. 1b, both curves exhibit a shoulder around 72 Å and a peak at 146 Å, and in fig. 2b, both show a shoulder around 80 Å and a peak at 138 Å.

Introduction of models B and D involves the postulation of the following mechanism for the process of dissociation. Native 48-mer comprising two layers, each of which has four submultiples, dissociates into two 24-mers composed of a single layer, as in the case of model D on removal of Ca^{2+} by using EDTA.

Model E: fitting of the model for the dodecamer (pH 5.0 in the presence of EDTA) was performed assuming that two submultiples (R_0 = 58 Å) are in contact with each other. The simulated curve is shown in fig. 4a, as is that obtained experimentally. The first shoulder (around 0.03 $Å^{-1}$) of the calculated curve appears less pronounced as compared to the experimental profile, but nevertheless does exist. The R_g value of the 12-mer model was estimated as 73.4 Å, the experimental result being 77.3 Å. The function $P(r)$ as evaluated for the 12-mer model shows a peak of 70 Å with a shoulder around 133 Å (fig. 4b). Although the shoulder on the experimental curve

appears less distinct, the simulation curve reproduces the experimental data reasonably well.

From models B, D and E, the values of R_g^3 were calculated to be in the ratio $1 : 1/1.5 : 1/3.0$. Comparison with the experimental ratio ($1 : 1/1.8 : 1/2.9$) shows the R_g values of models B and E to be in good agreement, whereas that of model D is larger. This implies that four submultiples of the 24-mer are arranged in a layer of two 12-mers, possibly twisted somewhat from the plane.

At pH 9 in the presence of 20 mM EDTA (D_3 state), the R_g value for the fragment was determined as 36.5 Å, which is less than that of a submultiple (44.9 Å), indicating that the submultiples are broken down into subunits, consistent with data from sedimentation analysis. We observed the experimental curve to be satisfactorily accounted for on fitting the model to a plot of log I vs h, taking a small sphere of radius 32 Å as the monomer subunit. The simulated curve is demonstrated in fig. 5a in addition to the experimental profile. Except for the range $h < 0.04$ Å^{-1}, the model provides a reasonable fit to the experimental data. The radius of gyration corresponding to this sphere amounts to 24.8 Å ($= \sqrt{3/5} \times 32$ Å). Since the R_g ratio (submultiple/small sphere) is 44.9/24.8, the cube of the ratio is close to 6 (5.9). This result is in support of the volume of the subunit at pH 9 in the presence of 20 mM EDTA being 1/6 of that of the submultiple, i.e., a monomer. Below $h = 0.04$ Å^{-1}, the experimental profile is slightly above the simulated curve. This difference might be due to the presence of very small amounts of oligomers arising from reassociation, which are supposed to represent less than a few percent of the total protein [2] and were, in fact, undetectable by sedimentation analysis. The function $P(r)$ was also simulated according to the model of the small sphere of radius 32 Å. As shown in fig. 5b, the agreement between the calculated and experimental curves is fairly good. The data therefore appear to support the contention that hemocyanin undergoes dissociation mainly into the constituent monomer, with 1/6 of the volume of the submultiple, at pH 9 in the presence of 20 mM EDTA in accordance with the results from ultracentrifugation.

3.3. Comparison of sizes of the dissociated fragments with the corresponding hemocyanins occurring in nature

From sedimentation analysis of *L. polyphemus* hemocyanin, Brenowitz et al. [2] established that the protein undergoes denaturation below pH 4 and dissociates into a mixture comprising the monomer above pH 7.8 in the presence of EDTA. Between pH 4.2 and 5.0, it exists in the form of dodecamers. Between pH 6.3 and 7.6, the 24-mer is the prevailing form in the presence of EDTA. The present SXS study is consistent with their results from the steric viewpoint and provides further appropriate models for native hemocyanin and dissociated fragments. On the other hand, Lamy et al. [1] proposed detailed models of arthropodan hemocyanins on the basis of molecular immunoelectron microscopy. Their models are considered to be essentially the same as ours, although the shape of the submultiple (hexameric building block) differs somewhat. Their hexameric building block, which is composed of six kidney-shaped subunits, is drum-shaped, in contrast to our spherical model.

On removal of Ca^{2+} by EDTA, the native hemocyanin (48-mer) comprising eight submultiples arranged in two superimposed tetragonal layers dissociates into two single layers (the half molecule, i.e., 24-mer). Lamy et al. [16] postulated the shape of the half molecule of *L. polyphemus* hemocyanin, based on the electron micrographs, to show the assembly of four submultiples into a rectangular solid. They proposed a 'flip-flop' model for *Androctonus australis* and *E. californicum* hemocyanins (24-mer) [1] which are composed of four hexameric building blocks assembled into a single layer. These hemocyanins cannot be distinguished on electron micrographs from the half molecule (24-mer) of *L. polyphemus* hemocyanin. The current SXS study also confirms the single layer structure of the half molecule (24-mer) of *L. polyphemus* in analogy with one of the double layers in native hemocyanins as a whole. It has also been demonstrated herein that the *Limulus* hemocyanin dissociates into two dimeric submultiples (12-mer) in accord with the electron microscopy study [17]. Pilz et al. [4] reported the

quaternary structure of *Astacus leptodactylus* hemocyanin (12-mer) as determined by SXS and postulated a detailed model constituted of 12 small spheres (subunits), assembled to form two submultiples. Their model appears to be in conformity with ours essentially with respect to the submultiple assembly. Thus, this hemocyanin is considered to have a structural hierarchy of the following order: monomer, 12-mer (dimer of the submultiple), 24-mer (tetramer of the submultiple), and 48-mer (octamer of the submultiple).

It is noteworthy that the stable hexamer (single submultiple) has never been found in the *Limulus* hemocyanin. This may be interpreted as follows. The hexamer is not stable enough to retain the quaternary structure and dissociates readily into subunits, differing from the native hexameric hemocyanin of *Panulirus interruptus*. Another possibility is that the submultiple cannot be broken down into hexamers due to the considerable strength of bonding between the two subunits assigned to the different hexamers in contact. Brenowitz et al. [18] have reported that subunits of *Limulus* hemocyanin form dimers (V-V and V′-VI), which are presumed to be tightly bound by the cross-links between two hexamers. In the present experiment, at pH 9.0, the hemocyanin molecule is supposed to dissociate mainly into the monomer and partly into the dimer without forming the hexamer, the absence of which may be attributed to the inter-hexamer bond remaining intact.

References

1 J.N. Lamy, J. Lamy, E. Billiad, P.Y. Sizaret, J.C. Taveau, N. Boisset, J. Frank and G. Motta, in: Invertebrate oxygen carriers, ed. B. Linzen (Springer, Berlin, 1986) p. 185.
2 M. Brenowitz, C. Bonaventura and J. Bonaventura, Biochemistry 233 (1984) 879.
3 I. Pilz, in: Small angle X-ray scattering, eds O. Glatter O. Kratky (Academic Press, London, 1982) p. 239.
4 I. Pilz, K. Goral, M. Hoylaerts, R. Witters and R. Lontie, Eur. J. Biochem. 105 (1980) 539.
5 J. Berger, I. Pilz, R. Witters and R. Lontie, Eur. J. Biochem. 80 (1977) 79.
6 I. Pilz, E. Schwarz, Y. Tsfadia and E. Daniel, Int. J. Biol. Macromol. 10 (1988) 353.
7 I. Pilz, E. Schwarz, T. Suzuki and T. Gotoh, Int. J. Biol. Macromol. 10 (1988) 356.
8 T. Nagamura, K. Kurita, E. Tokikura and H. Kihara, J. Biochem. Biophys. Methods 11 (1985) 277.
9 H. Tsuruta, T. Nagamura, K. Kimura, Y. Igarashi, A. Kajita, Z.-X. Wang, K. Wakabayashi, Y. Amemiya and H. Kihara, Rev. Sci. Instrum. 60 (1989) 2356.
10 M. Brouwer, C. Bonaventura and J. Bonaventura, Biochemistry 22 (1983) 4713.
11 Y. Amemiya, K. Wakabayashi, T. Hamanaka, T. Wakabayashi, T. Matsushita and H. Hashizume, Nuclear Instrum. Methods 208 (1983) 471.
12 A. Guinier and G. Fournet, Small-angle scattering of X-rays (Wiley, New York, 1955).
13 T. Furuno, A. Ikegami, H. Kihara, M. Yoshida and Y. Kagawa, J. Mol. Biol. 170 (1983) 137.
14 I. Pilz, O. Glatter and O. Kratky, Methods Enzymol. 61 (1979) 148.
15 Z.-X. Wang, H. Tsuruta, Y. Honda, Y. Tachi-iri, K. Wakabayashi, Y. Amemiya and H. Kihara, Biophys. Chem. 33 (1989) 153.
16 J. Lamy, P.-Y. Sizaret, J. Frank, A. Verchoor, R. Feldmann and J. Bonaventura, Biochemistry 21 (1982) 6825.
17 M.M.C. Bijlholt, E.F. van Bruggen and J. Bonaventura, Eur. J. Biochem. 95 (1979) 399.
18 M. Brenowitz, C. Bonaventura and J. Bonaventura, Arch. Biochem. Biophys. 230 (1984) 238.